Equation of state of metallic hydrogen from coupled electron-ion Monte Carlo simulations

Miguel A. Morales,[1,*] Carlo Pierleoni,[2,†] and D. M. Ceperley[3,‡]
[1]*Department of Physics, University of Illinois at Urbana-Champaign, Illinois 61801, USA*
[2]*Consorzio Nazionale Interuniversitario per le Scienze Fisiche della Materia and Physics Department, University of L'Aquila, Italy*
[3]*Department of Physics, National Center of Supercomputer Applications, and Institute of Condensed Matter Physics, University of Illinois at Urbana-Champaign, Illinois 61801, USA*

(Received 10 June 2009; revised manuscript received 19 January 2010; published 24 February 2010)

We present a study of hydrogen at pressures higher than molecular dissociation using the coupled electron-ion Monte Carlo method. These calculations use the accurate reptation quantum Monte Carlo method to estimate the electronic energy and pressure while doing a Monte Carlo simulation of the protons. In addition to presenting simulation results for the equation of state over a large region of the phase diagram, we report the free energy obtained by thermodynamic integration. We find very good agreement with density-functional theory based molecular-dynamics calculations for pressures beyond 600 GPa and densities above $\rho = 1.4$ g/cm^3, both for thermodynamic and structural properties. This agreement provides a strong support to the different approximations employed in the density-functional treatment of the system, specifically the approximate exchange-correlation potential and the use of pseudopotentials for the range of densities considered. We find disagreement with chemical models, which suggests that a reinvestigation of planetary models—previously constructed using the Saumon-Chabrier-Van Horn equations of state—might be needed.

DOI: 10.1103/PhysRevE.81.021202 PACS number(s): 61.20.Ja, 62.50.−p, 31.15.A−

I. INTRODUCTION

Although hydrogen is the first element in the Periodic Table, it undergoes a number of transformations as temperature and density are varied. As the most abundant element in the universe, it is important to have an accurate prediction of its properties for a large range of pressures and temperatures. A qualitative description is not always sufficient. For example, models of hydrogenic planets require accurate results to make correct predictions [1,2]. Estimates are that the equation of state (EOS) (the pressure as a function of density and temperature) needs to be accurate to 1% to answer fundamental questions about the composition and formation of the Jovian planets [3].

The high-pressure phases of hydrogen have received considerable attention in recent years, both from theory and experiment. At lower temperatures, static compression experiments using diamond-anvil cells can reach pressures of 320 GPa, where the quest to find the metal-insulator and molecular-atomic transitions in the solid phase still continues [4]. Dynamic compression experiments using either isentropic compression or shock waves are used at higher temperatures and can now reach pressures above 200 GPa [5,6]. Even though experimental techniques at high pressure have improved considerably over the last decade, they are still not accurate enough to measure the EOS to the required precision. Although this situation might change in the near future with the construction of more powerful machines such as the National Ignition Facility, computer simulations today provide the most reliable method for determining the thermodynamic properties at high pressures and temperatures.

Many theoretical techniques have been used including free-energy minimization methods in the chemical picture [7–9], restricted path integral Monte Carlo (PIMC) [10], and density-functional theory based molecular dynamics (DFT-MD) [11–17]. All of these methods employ different approximations that can affect properties in ways that are difficult to quantify due to the lack of conclusive experimental results. While free-energy methods are typically accurate in the molecular phase at low pressures, where molecules are tightly bound and there are enough experimental results to produce accurate empirical potentials, at higher density, with the onset of dissociation and metallization in the liquid, they become unreliable. These methods must interpolate between the low and high pressures (i.e. the plasma state). One expects possibly large errors at intermediate pressures, i.e., at conditions directly relevant to planetary interiors.

Restricted PIMC, on the other hand, is accurate at very high temperatures where the nodes of the density matrix are known, but at temperatures below approximately 20 000 K its accuracy (and efficiency) has been limited. For intermediate temperatures and high pressures, DFT-MD has become the computational method of choice over the last decade, mainly due to its advanced development stage and easy accessibility with many available packages. Practical implementations of DFT employ pseudopotentials and approximate exchange-correlation functionals and do not typically estimate quantum proton effects; these approximations limit its accuracy and applicability, especially at high pressures. Despite its possible limitations, DFT is a state of the art in *ab initio* simulations. For example, planetary models are being built with its equation of state, superseding the well-known Saumon-Chabrier-Van Horn (SCVH) multiphase equation of state [7,18].

Because of its widespread use and potential impact in the near future, it is important to test the validity of the DFT approximations at extreme conditions and to determine its range of applicability. In order to obtain more accurate re-

*mmorale3@illinois.edu
†carlo.pierleoni@aquila.infn.it
‡ceperley@illinois.edu

sults, especially at intermediate temperatures, we need to employ methods that can go beyond the usual single-body mean-field approximations typically used in DFT. Quantum Monte Carlo (QMC) is a perfect candidate for the task, presenting a good balance between speed and accuracy. It does not rely on pseudopotentials, and electronic correlation effects are treated explicitly in the full many-body problem. At present, QMC has the potential to be more accurate for electronic properties than DFT, while being considerably less expensive than correlated quantum chemistry methods [19–21].

Coupled electron-ion Monte Carlo (CEIMC) is a QMC based *ab initio* method devised to use QMC electronic energy in a Monte Carlo simulation of the ionic degrees of freedom [22,23]. Thanks to recent advances in QMC methodology we can now obtain results with small and well controlled systematic errors. Specifically, the use of twist averaged boundary conditions (TABCs) [24] on the phase of the electronic wave function, together with recently developed finite-size correction schemes [25,26], allows us to produce energies that are well converged to the thermodynamic limit with ~100 atoms; see Appendix A for additional details. Improvements in the wave functions used for high-pressure hydrogen allow us to get very accurate results [27] and avoid the main limitations of previous applications of the CEIMC method.

The impressive increase in computational power in recent years made possible a calculation of the EOS of hydrogen over a broad range of temperatures and pressures. In this paper we present the results of free-energy calculations of hydrogen in its atomic liquid phase for pressures greater than 150 GPa. In Sec. II, we present a brief description of the CEIMC method. In Sec. III we present the results for the EOS, including the free-energy calculations. In Sec. IV we present a comparison with other methods, with a special attention to DFT-MD results, while in Sec. V we draw some conclusions. Finally, in Appendixes A and B we describe details of the method to estimate the finite-size corrections and of the reptation quantum Monte Carlo (RQMC) method implemented in CEIMC, respectively.

II. COUPLED ELECTRON-ION MONTE CARLO METHOD

CEIMC, in common with the large majority of *ab initio* methods, is based on the Born-Oppenheimer (BO) separation of electronic and ionic degrees of freedom. In addition, the electrons are considered to be in their ground state for any particular arrangement of the protons. This approximation is well justified in the regime of the phase diagram studied here because the Fermi temperature for the electrons is well above 250 000 K. To estimate the electronic thermal effects on the thermodynamic properties we performed DFT simulations at a temperature of 10 000 K (the highest temperature reported in this work) and a density of 2.03 g/cm^3, using both ground-state and finite-temperature versions of DFT [28]. We obtained changes of 0.3%, 0.4%, and 2% for the pressure, Helmholtz free energy, and entropy of the liquid, respectively. Details of DFT simulations will be given below. As further support of the validity of the ground-state assumption, note that we have previously observed [29] a good agreement for the radial distribution functions (proton-proton, proton-electron, and electron-electron) between CEIMC and finite-temperature restricted PIMC at $r_s=1.0$ and $T=5000$ K. Protons, either considered as classical or quantum particles [23,29], are assumed to be at thermal equilibrium at a temperature T. In the present calculation, the system of N protons and N electrons is enclosed in a fixed volume V at a number density $n=N/V$, which we often express with the parameter $r_s=(3/4\pi n)^{(1/3)}$. The mass density is related to r_s by $\rho=(3m_h)/(4\pi r_s^3)$, with m_h as the mass of a hydrogen atom, which provides the following conversion formula: $\rho(g/cm^3)=2.696/r_s^3$.

We start from the nonrelativistic Hamiltonian

$$\hat{H}=-\sum_{i=1}^{2N}\frac{\hbar^2}{2m_i}\nabla_i^2+\frac{e^2}{2}\sum_{i\neq j}\frac{z_i z_j}{|\hat{\vec{r}}_i-\hat{\vec{r}}_j|}, \tag{1}$$

where z_i, m_i, and $\hat{\vec{r}}_i$ represent, respectively, the valence, mass, and position operators of particle i. Let us denote with $R=(\vec{r}_1,\ldots,\vec{r}_N)$ and $S=(\vec{r}_{N+1},\ldots,\vec{r}_{2N})$ the set of coordinates of all electrons and protons, respectively [30].

Within the BO approximation, the ground-state energy of the system for a given nuclear state S is the expectation value of the Hamiltonian $\hat{H}$ over the corresponding normalized exact ground state $|\Phi_0(S)\rangle$,

$$E_{BO}(S)=\langle\Phi_0(S)|\hat{H}|\Phi_0(S)\rangle, \tag{2}$$

which is a $3N$-dimensional integral over the electron coordinates in configuration space,

$$E_{BO}(S)=\int dR\Phi_0^*(R|S)\hat{H}(R,S)\Phi_0(R|S)$$

$$=\int dR|\Phi_0(R|S)|^2E_L(R|S), \tag{3}$$

with the *local energy* defined as

$$E_L(R|S)=\frac{\hat{H}(R,S)\Phi_0(R|S)}{\Phi_0(R|S)}. \tag{4}$$

In this work, we use RQMC [31] with the bounce algorithm [32] to solve the electronic problem.

For an isolated hydrogen molecule, the error of the BO energy is approximately 0.3 mhartree/atom [33], roughly $(m_e/m_p)E$. This is about the size of the statistical error in our most converged calculations (see Table I). Because these corrections arise from the perturbation $\langle\hbar^2/(2m_p)|\nabla_S\Phi_0(R,S)|^2\rangle$, we expect much smaller corrections in the atomic liquid or plasma state studied here since the electrons are less coupled with the protons, resulting in smaller gradients.

With the ability to compute the BO electronic energy, the METROPOLIS algorithm is able to generate a sequence of ionic states according to the Boltzmann distribution $P(S)\propto\exp[-\beta E_{BO}(S)]$ at the inverse temperature β. In CEIMC the estimate of $E_{BO}(S)$ for a given trial function is computed by QMC and it is therefore affected by statistical noise which, if

TABLE I. Energy per atom and pressure as calculated with CEIMC and with BOMD. Statistical errors are reported in parentheses as the uncertainty on the last digit.

Method			CEIMC		BOMD	
T (K)	ρ (g/cm^3)	r_s	Energy (hartree)	Pressure (GPa)	Energy (hartree)	Pressure (GPa)
2000	2.329	1.05	−0.3846(3)	1576(2)		
3000	2.329	1.05	−0.3777(2)	1607(1)		
4000	2.329	1.05	−0.3707(5)	1640(3)	−0.37438(5)	1635.4(4)
6000	2.329	1.05	−0.3569(4)	1701(2)	−0.3610(1)	1701.0(7)
8000	2.329	1.05	−0.3458(4)	1753(2)	−0.3484(1)	1762.4(7)
10000	2.329	1.05	−0.3316(8)	1814(4)	−0.3360(2)	1823(2)
2000	2.026	1.10	−0.4170(2)	1157(2)		
3000	2.026	1.10	−0.4097(2)	1190(1)		
4000	2.026	1.10	−0.4026(3)	1219(1)	−0.4059(1)	1218.7(7)
6000	2.026	1.10	−0.3898(4)	1270(2)	−0.3927(1)	1276.1(9)
8000	2.026	1.10	−0.3777(5)	1315(2)	−0.3804(1)	1328.8(6)
10000	2.026	1.10	−0.3660(4)	1362(2)	−0.3690(3)	1378(2)
2000	1.773	1.15	−0.4419(2)	861(1)		
3000	1.773	1.15	−0.4356(3)	883(2)		
4000	1.773	1.15	−0.4285(7)	911(3)	−0.43137(9)	916.5(3)
6000	1.773	1.15	−0.4151(6)	956(3)	−0.41883(7)	964.8(4)
8000	1.773	1.15	−0.4018(9)	1003(3)	−0.40686(8)	1010.1(5)
10000	1.773	1.15	−0.3891(8)	1048(2)	−0.39542(8)	1053.8(5)
2000	1.380	1.25	−0.4790(2)	482(1)		
3000	1.380	1.25	−0.4721(2)	501(1)		
4000	1.380	1.25	−0.4673(4)	514(2)	−0.46886(7)	528.0(4)
6000	1.380	1.25	−0.4549(6)	553(1)	−0.45675(9)	565.1(5)
8000	1.380	1.25	−0.4419(7)	588(3)	−0.4451(1)	600.4(6)
10000	1.380	1.25	−0.4324(7)	616(2)	−0.4344(1)	633.2(5)
2000	0.983	1.40	−0.5117(4)	213(1)		
3000	0.983	1.40	−0.5057(2)	220(1)		
4000	0.983	1.40	−0.4993(5)	232(1)	−0.50203(6)	241.9(3)
6000	0.983	1.40	−0.4869(5)	256(3)	−0.4905(1)	267.0(3)
8000	0.983	1.40	−0.4767(5)	275(1)	−0.4796(1)	291.6(3)
10000	0.983	1.40	−0.4674(4)	295(1)	−0.4692(1)	315.0(6)
2000	0.724	1.55	−0.5330(2)	111(1)		
3000	0.724	1.55	−0.5230(2)	105(1)		
4000	0.724	1.55	−0.5157(3)	116(1)		
6000	0.724	1.55	−0.5027(4)	134(1)		
8000	0.724	1.55	−0.4938(2)	143(1)		
10000	0.724	1.55	−0.4831(6)	162(2)		

ignored, will bias the result. In the penalty method [34], we require detailed balance to hold if averaged over the noise distribution. The noise on the energy difference causes extra rejection with respect to the noiseless case.

The accuracy of the calculations depends crucially on the choice of the trial wave function. The Slater-Jastrow wave function has the form

$$\Psi_T(R,S) = D_\uparrow D_\downarrow e^{-U}, \tag{5}$$

where $D_{\uparrow/\downarrow}$ is a Slater determinant of single-electron orbitals for electrons with spin up/down and U is the sum, over all distinct pairs of particles, of the random-phase approximation (RPA)-Jastrow function [22]. The orbitals in the Slater determinant are obtained from a DFT calculation in a plane-wave basis, using the local-density approximation for the exchange-correlation functional, as parametrized by Perdew and Zunger [35] and Ceperley and Alder [36]. The resulting orbitals are transformed to a cubic spline basis from which they are interpolated in the QMC calculations. The use of a spline basis in the RQMC runs represents a large increase in the efficiency of the simulations. To reduce the computational overhead produced by the DFT calculations, which

must be converged to self-consistency for every ionic step, we perform a single self-consistent DFT calculation at the Γ point of the supercell; in other words we assume that the orbitals are periodic in the supercell [37]. Using the resulting electron density, we build and diagonalize the Kohn-Sham Hamiltonian at the points in the Brillouin zone of the supercell required in the TABC calculations.

We apply a backflow transformation [38] to the electron coordinates in the Slater determinant with the form

$$\vec{x}_i = \vec{r}_i + \sum_j \eta_{ij}(|r_{ij}|)\vec{r}_{ij}, \tag{6}$$

where η is either a parametrized electron-electron backflow function or an analytical form derived using Bohm-Pines collective coordinate approach [39]. This introduces correlations and improves the nodal surfaces of the DFT orbitals [20,27,39]. This many-body wave function represents a good balance between accuracy and efficiency.

III. EQUATION OF STATE OF HYDROGEN

In this paper we calculate the free energy of hydrogen as a function of temperature and density for ranges $2000 < T < 10\,000$ K and $0.7 < \rho < 2.4$ g cm^{-3}. For $\rho < 0.7$ g cm^{-3}, molecular dissociation becomes the dominant feature in the EOS, requiring a more detailed study than the one performed here to reach a similar level of accuracy. Such simulations are in progress and will be reported elsewhere.

The CEIMC calculations were performed with 54 hydrogen atoms using RQMC. The time step and projection length used in RQMC were chosen to reach a convergence of the energy of 0.2–0.3 mhartree/atom; see Appendix B for details. We used TABC with a grid of 64 twists (96 for $r_s \leq 1.10$), which together with the use of recently developed finite-size correction schemes for QMC energies allows a significant reduction in size effects; see Appendix A for details and discussion.

We performed 36 CEIMC simulations [not including those related to the coupling constant integration (CCI)]; the results are reported in Table I. The initial proton configurations (typically associated with regular lattice arrangements) were first relaxed using effective pair potentials between protons, built from reflected Yukawa functions [see Eq. (8) below], which were chosen in such a way that they reproduce approximately the radial distribution functions of the QMC systems. We then performed 2000–3000 equilibration steps with CEIMC. Statistics were gathered in the following 5000–15 000 steps, with the number of steps depending on temperature and density.

The protons are treated as classical particles in the results presented in Table I and in the free-energy calculations discussed below. Quantum effects of the protons could be important at low temperatures at the densities considered in this work. In order to assess their effect on the thermodynamic properties, we performed PIMC calculations for the protons on the potential-energy surface defined by the zero-temperature RQMC method. This is an extension of CEIMC to treat quantum nuclei [23]. The resulting corrections to the energy and pressure are given in Table II, at $T=2000$ K for three densities. At this temperature, which is the lowest temperature studied in this work, the corrections to the pressure from quantum proton effects are limited to 1%.

TABLE II. Corrections to the energy and pressure of hydrogen from quantum effects of the protons, from PIMC simulations with CEIMC, at a temperature of 2000 K: $\Delta E=(E-E_{classical})/N$ and $\Delta P=P-P_{classical}$. Errors are in parentheses.

r_s	ΔE (mhartee)	ΔP (GPa)	$\Delta P/P$ (%)
1.05	4.0(7)	7(3)	0.4
1.10	3.8(3)	9(1)	0.7
1.25	2.8(5)	5(1)	1.0

A. Free-energy integration

We used CCI [40] to calculate the free energy of hydrogen at a reference point chosen as $T=6000$ K and $r_s=1.25$. In CCI a λ-dependent potential energy $V(\lambda)$ is a linear combination of two different potential energies: $V(\lambda)=V_0+\lambda(V_1-V_0)$. The difference in free energy between systems 0 and 1 is then

$$F_1 - F_0 = \int_0^1 d\lambda \langle (V_1 - V_0) \rangle_\lambda, \tag{7}$$

where $\langle \cdots \rangle_\lambda$ indicates a statistical average over the distribution $\sim e^{-\beta V(\lambda)}$. We chose system 0 to be a system of classical point particles with pairwise additive interaction of the Yukawa type,

$$v_0(r) = \begin{cases} \dfrac{e^{-br}}{r} + \dfrac{e^{-b(L-r)}}{(L-r)} - 4\dfrac{e^{-bL/2}}{L}, & r \leq L/2 \\ 0, & r > L/2, \end{cases} \tag{8}$$

where $b=2.5a_0^{-1}$ with a_0 being the Bohr radius and L is the length of the simulation cell. The reflection makes the function and its first derivative continuous at the cutoff, $r=L/2$. We performed a first CCI to compute the free energy of the effective system at the desired thermodynamic point using $V(\lambda)=\lambda V_0$, so that the effective system was transformed into an ideal system. A second CCI was performed to switch the effective system into the system of classical protons and ground-state electrons and therefore evaluate the free energy of hydrogen at the reference point. In this second CCI we used $V(\lambda)=\lambda V_0+(1-\lambda)E_{BO}(\lambda)$, where $E_{BO}(\lambda)$ is the Born-Oppenheimer energy as obtained from RQMC. Note that E_{BO} depends implicitly on the specific value of λ, a dependence that we have explicitly indicated. We obtained a value of −0.5737(1) hartree/atom for the free energy and 6.25(3) (k_B/atom) for the entropy at the reference point. The free energy at thermodynamic points other than the reference point was obtained by thermodynamic integration [41], i.e., integrating the internal energy or the pressure along, respectively, isochors or isotherms of the system.

TABLE III. Coefficients of the expansion of the free energy; energy is in hartree/atom, temperature is in K, and density is in g cm^{-3}.

k	c_{1k}	c_{2k}	c_{3k}	c_{4k}
1	−0.529586	-2.085591×10^{-4}	-3.365628×10^{-9}	2.294411×10^{-5}
2	2.227221×10^{-6}	-1.452601×10^{-4}	-2.488880×10^{-9}	1.894880×10^{-5}
3	-6.266619×10^{-5}	4.210279×10^{-4}	6.174066×10^{-9}	-5.144879×10^{-5}
4	9.977346×10^{-2}	-6.220508×10^{-4}	-8.564851×10^{-9}	7.499558×10^{-5}
5	-1.437627×10^{-2}	-9.867541×10^{-5}	-1.598083×10^{-9}	1.225739×10^{-5}

B. Fits to EOS

The free energy as a function of temperature and density was parametrized by the functional form

$$F(T,\rho)=\sum_{i=1}^{4}\sum_{k=1}^{5}c_{ik}g_i(T)g_k(\rho), \tag{9}$$

where $g_i(x)=\{1,x,x^2,x\ln x,x^2\ln x\}$. The parameters c_{ik} were determined by a least-squares fit to CEIMC data for energy and pressure of the analytical derivatives of this expansion,

$$P(T,\rho)=\frac{\rho^2}{m_h}\left(\frac{\partial F}{\partial\rho}\right)_T, \tag{10}$$

$$E(T,\rho)=-T^2\left[\frac{\partial}{\partial T}\left(\frac{F}{T}\right)\right]_\rho. \tag{11}$$

The free-energy fit reproduces the energies and pressures obtained from the CEIMC simulations to within 0.5% and 1.5%, respectively, although the average error is much smaller than this. The coefficients of the expansion are given in Table III.

IV. COMPARISON WITH OTHER METHODS

In order to asses the accuracy of the DFT-MD method for hydrogen at such extreme conditions we have performed DFT based Born-Oppenheimer molecular dynamics (BOMD). As in the CEIMC calculations of the previous section, the electrons are assumed to be at zero temperature. The BOMD simulations were performed in the *NVT* ensemble (weakly coupled with a Berendsen thermostat) using the QBOX code [42]. We used the Perdew-Burke-Ernzerhof exchange-correlation functional and a Hamann-type [43] local pseudopotential with a core radius of $r_c=0.3$ a.u. to represent hydrogen. The simulations were performed with 250 hydrogen atoms in a cubic box using a plane-wave cutoff of 90 Ry (115 Ry for $r_s\geq1.10$) with periodic boundary conditions (Γ point of the simulation cell). Corrections to the EOS were added to extrapolate results to infinite cutoff and to account for the Brillouin-zone integration. To do this, we studied 15–20 statistically independent static configurations of protons at each density by using a $4\times4\times4$ grid of k points with a plane-wave cutoff of at least 300 Ry. See Ref. [44] for additional details of the BOMD simulations.

Data for energy and pressure obtained by CEIMC and BOMD are reported in Table I. There is a good agreement between the two methods, especially at higher densities where the difference in pressure is within error bars. Figure 1 shows a comparison of the pressure and the energy between CEIMC simulations and BOMD simulations. At lower densities, the pressure difference increases, reaching an average value of 5% close to the dissociation regime ($\rho\lesssim0.75$ g/cm^3). There is less reason to expect good agreement for the energies since DFT uses pseudopotentials and approximate exchange-correlation functionals which can modify the zero of the energy. However, the temperature and density dependence is well reproduced with an almost uniform energy shift of 0.8% in the region of the phase diagram studied. Figure 2 shows the proton-proton radial distribution function for several thermodynamic conditions as obtained with the two methods. The observed agreement is again remarkable. Note that the small wiggles in the CEIMC determined radial distribution function (r.d.f.) are statistical noise. The CEIMC functions were computed from fewer many-body configurations because of the greater computational

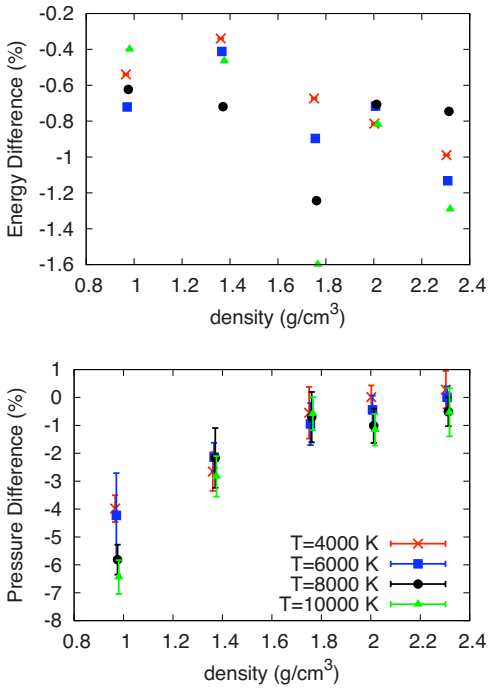

FIG. 1. (Color online) Comparison of energy and pressure between CEIMC and DFT-based BOMD simulations. We show the percent difference, defined as $\Delta A=\{(A_{CEIMC}-A_{BOMD})/[(A_{CEIMC}+A_{BOMD})/2]\}\times100$.

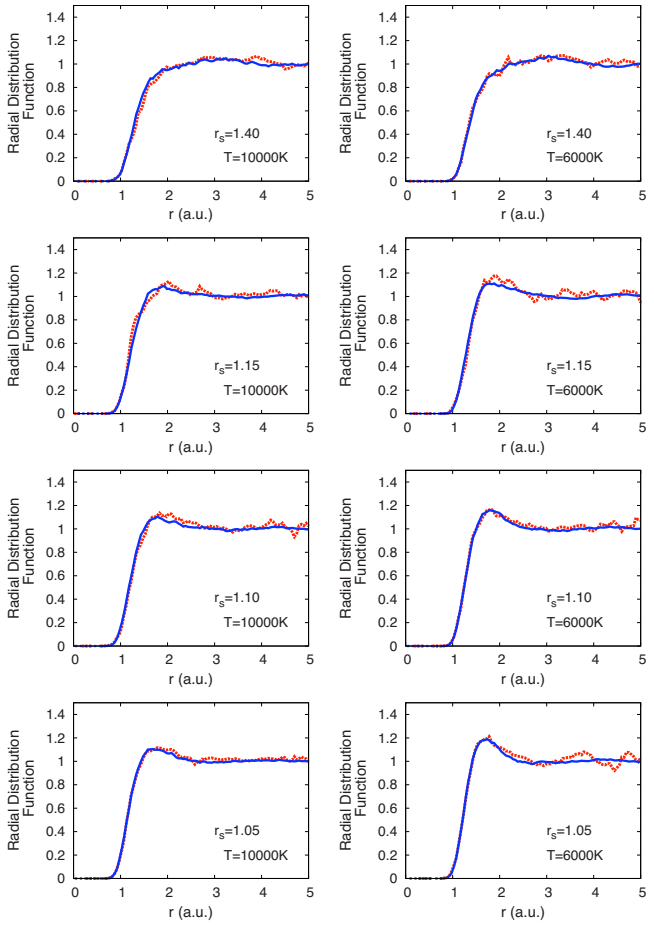

FIG. 2. (Color online) Comparison of radial distribution functions between BOMD (solid blue curve) and CEIMC (dashed red curve).

burden of QMC and thus have larger noise. The structure of the liquid is reproduced by BOMD simulations quite accurately, even the short-range correlation peak that develops at the lower temperatures and higher densities. Figure 3 shows a comparison for the entropy as a function of density along two isotherms. For densities beyond $\rho=1.4$ g/cm^3, the entropy curves obtained with the two methods are indistinguishable. In general, we obtain very good agreement between the two methods for pressures beyond 600 GPa. At lower pressures, the agreement is not perfect, but still very

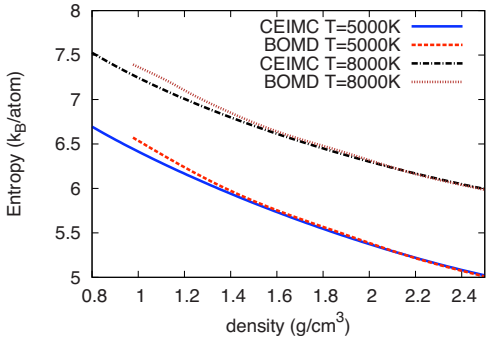

FIG. 3. (Color online) The entropy per atom at 5000 and 8000 K as determined with BOMD and CEIMC.

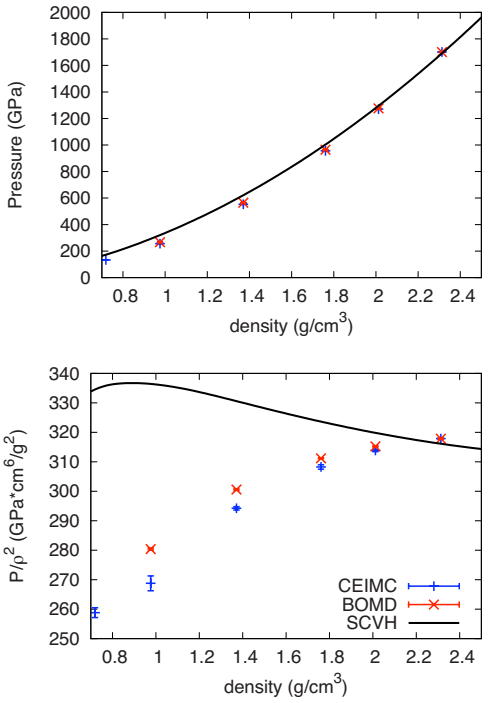

FIG. 4. (Color online) Comparison of pressure as a function of density computed with SCVH, BOMD, and CEIMC at $T=6000$ K. In the lower panel, the pressure is divided by ρ^2 to emphasize the differences.

good, with BOMD predicting a slightly higher entropy than CEIMC. We are currently expanding our calculations to lower density to provide an additional benchmark of the DFT method close to the molecular dissociation region.

Finally, Fig. 4 shows a comparison of the pressure as a function of density, obtained with CEIMC, BOMD, and the "interpolated" SCVH EOS at $T=6000$ K. The lower panel shows the pressure divided by the square of the density to highlight the differences between the results of the different methods. At pressures well below the dissociation regime (outside the regime investigated in the present work), SCVH EOS produces good results, but at higher densities, but still keeping the temperature $T\leq 10\,000$ K, the model is less accurate. As shown in Fig. 4 the SCVH pressures are 25% larger than those of CEIMC and BOMD.

The SCVH EOS is based on a chemical model of hydrogen, where one assumes dense hydrogen consists of H_2, H, e^-, and p^+ particles. The free energy is calculated assuming pair interactions between these species, and electronic excitations of the H atoms. In the CEIMC simulations there are, in fact, very few H_2 molecules and the atoms are strongly coupled (as evidenced by the r.d.f.) but incompletely ionized. In fact, one of the main limitations of the SCVH model is the lack of dependence of the H atom excitation energy on the surrounding plasma. As a consequence, the existence of bound states essentially determines that ionization takes place with a first-order plasma phase transition (PPT) rather than as a crossover [2]. In the SCVH model, the PPT is estimated to occur at ~ 0.5 g/cm^3 at 6000 K, but according to later work, such a prediction "is not credible" [2]. In the chemical model, in fact, there is a second spurious phase

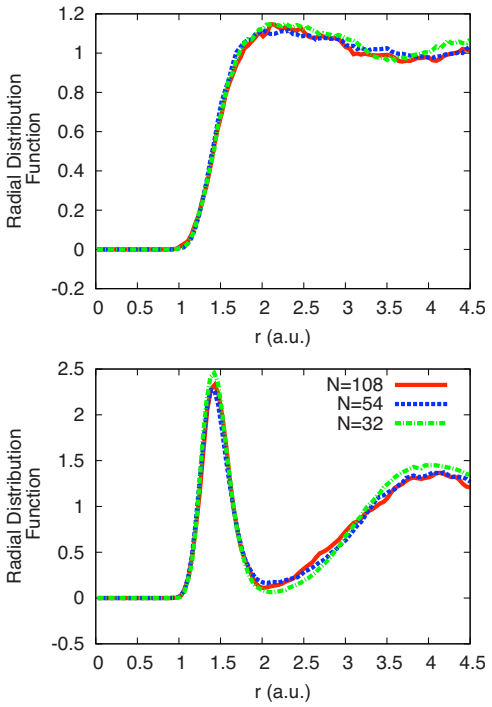

FIG. 5. (Color online) Comparison of proton-proton radial distribution functions between systems with different numbers of electrons. In the upper panel, the temperature is 4000 K and $r_s=1.25$. In the lower panel, the temperature is 3000 K and $r_s=1.85$. Electronic energies in CEIMC were calculated using variational Monte Carlo.

transition described as a "flaw in the EOS" at slightly higher temperatures and densities. This transition and the PPT are typically removed by smoothing out the free energy by hand. Based on CEIMC and BOMD calculations [45], the actual PPT should occur only at considerably lower temperatures: at 6000 K there should be a smooth crossover from H_2 to an atomic liquid. Hence, the errors in SCVH in this range of temperatures and pressures are likely due to effects of the interpolation. Although the errors in the SCVH are only observed to be large in a small portion of the temperature-density range of the model, this region is crucial for calculating the internal structure of Jupiter, in particular the size of the core region [2].

V. CONCLUSIONS

In summary, we performed a comprehensive study of the free energy and the equation of state of warm dense liquid hydrogen in its atomic phase using energies computed with a quantum Monte Carlo method. After performing finite-size corrections and estimating effects of zero-point proton energies, energies and pressures are computed to an absolute accuracy of a few percent. The free energy is computed using coupling constant and thermodynamic integrations. We provide a fit to the free energy which can be used as an input to models of the Jovian planets. The energies and pressures (Table I) can be used to constrain chemical models.

Given the status of DFT as a workhorse for EOS modeling, it is crucial to benchmark its predictions against more accurate correlated methods. We provide such a critical test at the conditions relevant for planetary interiors. Our results indicate that DFT based BOMD simulations provide a very good description of both thermodynamic and structural properties of hydrogen for $2000 \leq T \leq 10\,000$ K and densities of $0.7 \leq \rho \leq 2.4$ g cm^{-3} with errors in the total energy and pressures of less than 2%, except at densities of less than 1 g cm^{-3}, where DFT pressures are too high by 5%. With current day computer algorithms and capabilities, EOS calculations for hydrogen with a 1% accuracy are close to being achieved.

The equation of state of SCVH, used in the study of planetary interiors for more than a decade, is shown to produce pressures in error by 25% in this regime. We speculate that the errors in the SCVH are due to an inaccurate modeling of the molecular-atomic (i.e., PPT) transition, which is predicted to occur at a lower densities, but whose effect in the EOS extends up to conditions investigated here. Because planetary models are sensitive to details in this regime and at lower pressures during dissociation, a deviation from SCVH will produce a much larger change in the planetary model, e.g., it is found using a less compressible EOS that Jupiter has a core mass of 14–18 earth masses, much larger than SCVH value of 0–7 earth masses [1,18]. This suggests that planetary models, particularly of Jupiter, should be reinvestigated with a more accurate EOS, such as the one presented in this work.

ACKNOWLEDGMENTS

We thank M. Holzmann for useful discussions on the finite-size corrections. M.A.M. acknowledges support from the SSGF program, DOE Grant No. DE-FG52-06NA26170. C.P. thanks the Institute of Condensed Matter Theory at the University of Illinois at Urbana–Champaign and acknowledges financial support from Ministero dell'Università e della Ricerca Grant No. PRIN2007. The computer time was provided by the NCCS at Oak Ridge, Tennessee through the DOE INCITE program, and by CINECA at Bologna, Italy, through a CNISM grant.

APPENDIX A: FINITE-SIZE EFFECTS

Due to the high computational demands of QMC, our simulations are restricted to systems of at most 128 atoms. Many techniques have been developed in order to obtain useful results with finite systems. In this work we use TABC (the generalization of Brillouin-zone integration to many-body quantum systems in periodic boundary conditions) to eliminate shell effects in the kinetic energy of metallic systems. Twisted boundary conditions when an electron wraps around the simulation box are defined by

$$\Psi_\theta(\ldots,\vec{r}_j+\vec{L},\ldots)=e^{i\theta}\Psi_\theta(\ldots,\vec{r}_j,\ldots). \tag{A1}$$

where Ψ_θ is the many-body wave function of the system. Observables are then averaged over the all twist vectors, similar to one-body theories,

$$\langle \hat{A} \rangle = \int_{-\pi}^{\pi} \frac{d\vec{\theta}}{(2\pi)^3} \langle \Psi_\theta | \hat{A} | \Psi_\theta \rangle. \quad \text{(A2)}$$

This procedure has been shown to restore the classical $1/N$ dependence of the energy per particle in QMC calculations, absent when periodic boundary conditions (PBCs) are used [24].

As first shown by Chiesa *et al.* [25], most of the remaining finite-size errors in the potential and kinetic BO energies of QMC simulations come from discretization errors induced by the use of PBC. To see this, notice that we can write the potential energy (per electron) of a system of N electrons and N protons as

$$\frac{\langle \hat{V} \rangle}{N} = \frac{1}{2\Omega} \sum_{\vec{k} \neq 0} v(\vec{k}) [S_N(\vec{k}) - 2], \quad \text{(A3)}$$

where Ω is the volume of the simulation box, $\{\vec{k}\}$ is the set of lattice vectors in reciprocal space of the simulation box, $v(\vec{k})$ is the Fourier transform of the Coulomb potential, $S_N(\vec{k}) = \langle [\rho^p(\vec{k}) - \rho^e(\vec{k})][\rho^p(-\vec{k}) - \rho^e(-\vec{k})] \rangle / N$ is the charged structure factor, and $\rho^{p/e}(\vec{k}) = \Sigma_i e^{i\vec{k}\cdot\vec{r}_i}$; the sum over i refers to either protons or electrons depending on the superscript. As we approach the thermodynamic limit $N \to \infty$, the structure factor converges $[S_N(\vec{k}) \to S_\infty(\vec{k})]$ and the sum becomes an integral: $\frac{1}{\Omega} \Sigma_{\vec{k} \neq 0} \to \int d\vec{k}/(2\pi)^3$. Assuming, as it is usually the case, that the structure factor converges fast with the number of particles, then most of the finite-size error in the potential energy comes from the omission of the $\vec{k}=0$ term in the sum. This can be estimated using the Poisson summation formula

$$\int \frac{d\vec{k}}{(2\pi)^3} \hat{\eta}(\vec{k}) - \sum_{\vec{k} \neq 0} \hat{\eta}(\vec{k}) = \eta(0) - \sum_{\vec{L}} \eta(\vec{L}), \quad \text{(A4)}$$

where $\eta(r)$ is any generic position-dependent property of the periodic system and $\hat{\eta}$ is its Fourier transform. From the RPA, exact in the limit of $\vec{k} \to 0$, we know that $S_N(\vec{k}) \approx k^2$ as $k \to 0$. The leading-order correction to the potential energy per particle is

$$\delta V = \frac{3}{2Nr_s^3} \lim_{\vec{k} \to 0} \frac{S_N(\vec{k})}{k^2}. \quad \text{(A5)}$$

Computing the structure factor for small k during our simulation and extrapolating its behavior to $k=0$, we obtain the desired corrections. In the case of the electronic kinetic energy, following a similar argument, we obtain for the correction up to second order [25,26]

$$\delta K = \int \frac{d\vec{k}}{(2\pi)^3} \hat{u}(\vec{k}) k^2 - \frac{1}{\Omega} \sum_{\vec{k} \neq 0} \hat{u}(\vec{k}) k^2 = \frac{\sqrt{3}}{4Nr_s^{3/2}} - \frac{5.264}{2\pi r_s^2 (2N)^{4/3}}, \quad \text{(A6)}$$

where $\hat{u}(\vec{k})$ is the Fourier transform of electron-electron Jastrow function; in the present work we have used the RPA form [22].

To check the finite-size corrections [Eqs. (A5) and (A6)] for dense hydrogen, we performed simulations with 32, 54, and 108 atoms at $r_s = 1.85$ and 1.25. We used TABC with variational Monte Carlo energies with 108 twists for the 32-atom system and 32 twists for the 54 and 108 atoms. Figure 5 shows a comparison of the radial distribution functions between the systems with different numbers of atoms, for the two densities studied. Note that the two systems are very different: while the system at $r_s = 1.25$ and $T = 4000$ K is metallic, fully ionized plasma, the system at $r_s = 1.85$ and $T = 3000$ K exhibits a clear molecular character and is in the insulating phase [46]. For both systems, the agreement between the three simulations is very good, with no noticeable difference between the systems with 54 and 108 atoms validating the assumption that $S_N(k)$ is converged beyond 54 atoms. Using the fact that TABC restores the $1/N$ dependence of the properties, we can compare the results of the size correction formulas with a $1/N$ extrapolation. Table IV shows a comparison of finite-size corrections taking the system with 54 atoms as the reference. As can be seen, the correction for the lower-density system agrees very well with the extrapolated value. In the case of the higher-density system, the agreement is less good but still acceptable. We attribute the disagreement at higher densities to the differences in TABC used for the systems with different sizes.

TABLE IV. Comparison of finite-size corrections between a size extrapolation ($\Delta E_N, \Delta P_N$) and formulas (A5) and (A6) ($\Delta E_S, \Delta P_S$).

	Energy (mhartree)		Pressure (GPa)	
r_s	ΔE_N	ΔE_S	ΔP_N	ΔP_S
1.25	7.7	10.0	10.8	17.6
1.85	5.4	5.5	3.3	3.1

APPENDIX B: DETAILS OF RQMC CALCULATIONS

As mentioned in the text, the parameters of the RQMC calculations were varied with density to obtain uniform accuracy over the region of phase diagram investigated. Table V shows the time steps and projection times versus density used in the simulations. As is well known, total energies converge faster as a function of imaginary time because their convergence error is second order with respect to the trial wave function. The kinetic and potential energies, and hence

TABLE V. Projection time and time step used in the RQMC calculations.

r_s	Projection time (a.u.)	Time step (a.u.)
1.05	0.456	0.008
1.10	0.504	0.008
1.15	0.550	0.01
1.25	0.660	0.012
1.40	0.732	0.012
1.55	0.975	0.015

the pressure, obtained from the virial expression are only first order, which means that longer projection times are needed to obtain converged results. During the course of the simulations, we only require accurate energies, so a smaller projection time is used, one that is insufficient for accurate pressures. In order to obtain converged results for the pressure, we calculated a correction for the finite projection time and nonzero time step by studying approximately a dozen protonic configurations at each density. The corrections were found to be independent of the precise proton configuration but density dependent. The corrections to the total energy are negligible within errors.

[1] T. Guillot, Annu. Rev. Earth Planet Sci. **33**, 493 (2005).
[2] G. Chabrier, D. Saumon, and C. Winisdoerffer, Astrophys. Space Sci. **307**, 263 (2007).
[3] D. J. Stevenson (private communication).
[4] P. Loubeyre, F. Occelli, and R. LeToullec, Nature (London) **416**, 613 (2002).
[5] D. G. Hicks, T. R. Boehly, P. M. Celliers, J. H. Eggert, S. J. Moon, D. D. Meyerhofer, and G. W. Collins, Phys. Rev. B **79**, 014112 (2009).
[6] W. J. Nellis, Rep. Prog. Phys. **69**, 1479 (2006).
[7] D. Saumon, G. Chabrier, and H. M. Van Horn, Astrophys. J., Suppl. Ser. **99**, 713 (1995).
[8] G. I. Kerley, Phys. Earth Planet. Inter. **6**, 78 (1972).
[9] R. Redmer, B. Holst, H. Juranek, N. Nettelmann, and V. Schwarz, J. Phys. A **39**, 4479 (2006).
[10] B. Militzer and D. M. Ceperley, Phys. Rev. Lett. **85**, 1890 (2000).
[11] T. J. Lenosky, S. R. Bickham, J. D. Kress, and L. A. Collins, Phys. Rev. B **61**, 1 (2000); L. A. Collins *et al.*, *ibid.* **63**, 184110 (2001).
[12] M. P. Desjarlais, Phys. Rev. B **68**, 064204 (2003).
[13] S. Scandolo, Proc. Natl. Acad. Sci. U.S.A. **100**, 3051 (2003).
[14] S. A. Bonev, B. Militzer, and G. Galli, Phys. Rev. B **69**, 014101 (2004).
[15] S. A. Bonev, E. Schwegler, T. Ogitsu, and G. Galli, Nature (London) **431**, 669 (2004).
[16] J. Vorberger, I. Tamblyn, B. Militzer, and S. A. Bonev, Phys. Rev. B **75**, 024206 (2007).
[17] B. Holst, R. Redmer, and M. P. Desjarlais, Phys. Rev. B **77**, 184201 (2008).
[18] B. Militzer, W. B. Hubbard, J. Vorberger, I. Tamblyn, and S. A. Bonev, Astrophys. J. Lett. **688**, L45 (2008).
[19] C. J. Umrigar, J. Toulouse, C. Filippi, S. Sorella, and R. G. Hennig, Phys. Rev. Lett. **98**, 110201 (2007).
[20] P. Lopez Rios, A. Ma, N. D. Drummond, M. D. Towler, and R. J. Needs, Phys. Rev. E **74**, 066701 (2006).
[21] J. C. Grossman, M. Rohlfing, L. Mitas, S. G. Louie, and M. L. Cohen, Phys. Rev. Lett. **86**, 472 (2001).
[22] D. M. Ceperley, M. Dewing, and C. Pierleoni, Lect. Notes Phys. **605**, 473 (2002).
[23] C. Pierleoni and D. M. Ceperley, Lect. Notes Phys. **703**, 641 (2006).
[24] C. Lin, F. H. Zong, and D. M. Ceperley, Phys. Rev. E **64**, 016702 (2001).
[25] S. Chiesa, D. M. Ceperley, R. M. Martin, and M. Holzmann, Phys. Rev. Lett. **97**, 076404 (2006).
[26] N. D. Drummond, R. J. Needs, A. Sorouri, and W. M. C. Foulkes, Phys. Rev. B **78**, 125106 (2008).
[27] C. Pierleoni, K. T. Delaney, M. A. Morales, D. M. Ceperley, and M. Holzmann, Comput. Phys. Commun. **179**, 89 (2008).
[28] N. D. Mermin, Phys. Rev. **137**, A1441 (1965).
[29] C. Pierleoni, D. M. Ceperley, and M. Holzmann, Phys. Rev. Lett. **93**, 146402 (2004).
[30] We restrict the discussion to spin-unpolarized systems, i.e., systems with a vanishing projection of the total spin along any given direction, say $S_z=0$.
[31] S. Baroni and S. Moroni, Phys. Rev. Lett. **82**, 4745 (1999).
[32] C. Pierleoni and D. M. Ceperley, ChemPhysChem **6**, 1872 (2005).
[33] W. Kolos and L. Wolniewicz, J. Chem. Phys. **41**, 3663 (1964).
[34] D. M. Ceperley and M. Dewing, J. Chem. Phys. **110**, 9812 (1999).
[35] J. P. Perdew and A. Zunger, Phys. Rev. B **23**, 5048 (1981).
[36] D. M. Ceperley and B. J. Alder, Phys. Rev. Lett. **45**, 566 (1980).
[37] Even for a liquid, one has to specify the boundary conditions on the electronic wave function. Twist averaged BC means that one integrates over all possible boundary conditions on the phase of the wave function. For delocalized electrons, this results in much improved convergence to the large-N limit. If periodic boundary conditions are assumed, this corresponds to the Γ point of the Brillouin zone of the supercell.
[38] Y. Kwon, D. M. Ceperley, and R. M. Martin, Phys. Rev. B **48**, 12037 (1993).
[39] M. Holzmann, D. M. Ceperley, C. Pierleoni, and K. Esler, Phys. Rev. E **68**, 046707 (2003).
[40] J. G. Kirkwood, J. Chem. Phys. **3**, 300 (1935).
[41] D. Frenkel and B. Smit, *Understanding Molecular Simulations: From Algorithms to Applications*, 2nd ed. (Academic Press, San Diego, 2002).
[42] http://eslab.ucdavis.edu/software/qbox
[43] D. R. Hamann, Phys. Rev. B **40**, 2980 (1989).
[44] M. A. Morales, E. Schwegler, D. Ceperley, C. Pierleoni, S. Hamel, and K. Caspersen, Proc. Natl. Acad. Sci. U.S.A. **106**, 1324 (2009).
[45] M. A. Morales, C. Pierleoni, E. Schwegler, and D. Ceperley (unpublished).
[46] F. Lin, M. A. Morales, K. T. Delaney, C. Pierleoni, R. M. Martin, and D. M. Ceperley, Phys. Rev. Lett. **103**, 256401 (2009).